IOP Publishing | The Japan Society of Fluid Mechanics Fluid Dynamics Research

Fluid Dyn. Res. **52** (2020) 1–17 (17pp) https://doi.org/10.1088/1873-7005/ab9b62

# The effect of a parallel free surface upon a submerged shallow synthetic jet

**Abhay Kumar and Ashish Karn**

Department of Mechanical Engineering, University of Petroleum and Energy Studies, Energy Acres, Bidholi, Dehradun, Uttarakhand 248007, India

E-mail: akarn@ddn.upes.ac.in

Received 28 November 2019; revised 18 April 2020
Accepted for publication 10 June 2020
Published 13 August 2020

**Abstract**

The interaction of a submerged shallow synthetic jet with a parallel free surface has gathered substantial interest, owing to its relevance to the operation of marine vehicles viz. ships that move close to the water surface. However, despite exhaustive research on the perturbation on a free surface, very few studies have experimentally investigated the effect of unconfined water surface height on the evolution and propagation of a submerged synthetic jet. This study experimentally investigates a synthetic jet submerged in a quiescent flow at shallow depths ejecting parallel to the free surface, through qualitative analysis and quantitative measurements. The qualitative study includes the visualization of the flow using plane laser induced fluorescence (PLIF) technique, whereas the velocity measurements are carried out by a five-beam laser Doppler velocimetry (LDV) probe. The primary objective of these analysis and measurements is to gain a physical insight into the characteristics of vortex ring in a synthetic jet ejected from a fixed orifice at different water depths and at varying Reynolds number. Our studies indicate that the behavior of the vortex rings drastically changes as the depth of the jet crosses a certain threshold. Although no significant change in the path of synthetic jet is observed beyond a threshold depth in our experiments, the jet trajectory shows an interesting dependence on the Reynolds number based on circulation for shallow water depths. It has been found that at the shallow depths, the vortex ring drifts upwards and interacts with the free surface at lower Reynolds number, whereas for larger Reynolds number, the vortex ring rebounds near the free surface and moves downward. Based on our observations, it can be concluded that the phenomenon of upward/downward flection of vortex rings depends both upon its circulation and ejection depth.

Keywords: synthetic jet, submerged jet, vortex rings, LDV, PLIF

(Some figures may appear in colour only in the online journal)

  

## 1. Introduction

A synthetic jet can be defined as a train of vortex ring that originates completely from the working fluid, carries no net mass flux and yet transfers linear momentum to the fluid flow (Mohseni and Mittal 2015). Figure 1 shows the process of a synthetic jet actuation. As the vortex ring assisted by its self-effected velocity, moves downstream and interacts with the fluid, it enlarges till a point the energy of the circulation is unable to hold its growing size, eventually leading to its breakup into smaller pieces. As shown in the figure, a synthetic jet actuation system is usually constituted of an oscillating diaphragm, a cavity opening and a fixed boundary that encloses to form a cavity. The oscillations of the diaphragm are created at one end of the cavity, while the other end consists of an orifice. The diaphragm oscillations regulate the fluid suction and ejection rates through the orifice.

Synthetic jets are widely used in the industrial applications such as flow separation control over bluff bodies (Amitay *et al* 2004, Feng and Wang 2012), stalled airfoils (Amitay *et al* 2001) and in duct flows (Amitay *et al* 2002, Glezer *et al* 2005). (Fung and Amitay 2002) and (Jagadeesh *et al* 2009) have used synthetic jet with a view to control and maneuver the unmanned aerial vehicles. However, the manoeuvring (particularly at reduced speeds) and docking strategies of autonomous or remotely operated underwater vehicles are more challenging and a compact zero-mass pulsatile jet also known *as synthetic jet actuators* can be used (Linden and Turner 2004, De Luca *et al* 2014, Gil and Strzelczyk 2016). These synthetic jets have attracted much attention because although the distant field behaviour of a synthetic jet is very much identical to that of a continuous jet, it has many other advantages over a continuous jet. The most notable benefit of a synthetic jet as compared to a plain jet is that there is a supply of momentum at no net mass flux. Since the suction and ejection mass flow rates induced by the diaphragm are exactly identical, no net mass flow of fluid occurs. This absence of net mass flux obviates the need for any additional pumping fluid, pump, moving components such as valves, piston etc. In addition, experiments carried out on circular synthetic jets have demonstrated that the vortex pairs predominate in the vicinity of the synthetic jet (Kumar and Karn 2018). These vortex pairs entrain more fluid from surroundings and along with a larger volume flux, a synthetic jet also widens more swiftly in comparison to a continuous jet (Swift and Swift 2003). Other applications of synthetic jets have also been reported, such as jet-vectoring (Smith and Glezer 2002), electronic cooling (Pavlova and Amitay 2006, Travnicek *et al* 2011, Mcguinn *et al* 2013) and in mixing enhancement (Freund and Moin 2000, Al-Atabi 2011). The applications of synthetic jets in cross-flow have also been reported in boundary layer control and drag reduction (Lardeau and Leschziner 2011, Laouedj *et al* 2015, Buren *et al* 2016, Kumar and Karn 2018).

Among the different applications of synthetic jets, there are many potential situations where the synthetic jet comes near to the unconfined surface, i.e. in the shallow water depths. It is well known that the interaction of a jet and an unrestrained surface occurs in a plethora of environmental and geophysical flows, as well as in many technological applications. For instance, a typical example of a shallow jet—free surface association can be observed in the wake of a cruising ship. The cruising ships sailing in the ocean generate a hydrodynamic signature in its wake and the detection of this wake is crucial in tracing the trajectory of the ship over time. The synthetic jet in such shallow water depths can alter the wake signature of these ships, and thus may prove beneficial for naval defense applications. Typically, a shallow jet is bound by an unrestrained surface above and a solid wall at the bottom and spans to an unlimited horizontal extent in the transverse direction. A lot of research has already been reported in the area

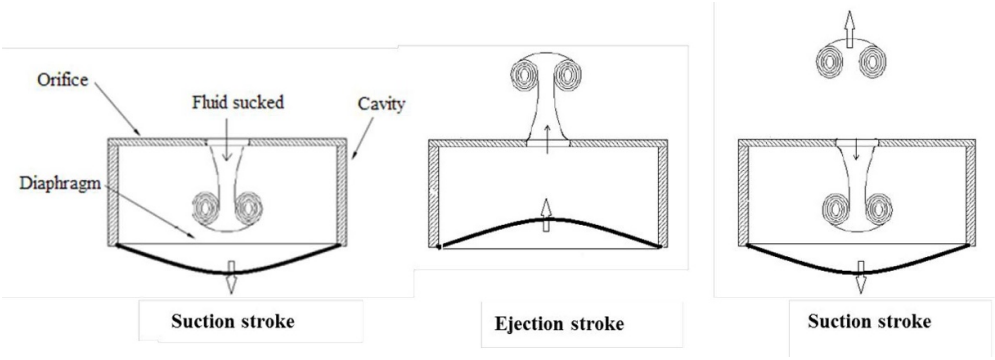


**Figure 1.** Schematic of a synthetic jet actuation using orifice-diaphragm apparatus.

of shallow jets. For instance, the work of (Rodi 1982) has established that the shallow water conditions have a significant impact on mixing of a jet and its entrainment due to restricted extent of the presence of ambient fluid above and below the jet. On a similar note, (Shinneeb *et al* 2011) has substantiated that the variation in average velocity and turbulence statistics depends on the depth of jet from the free surface and confinement in lateral direction of jet expansion for an isothermal round jet in shallow waters. The implications of shallowness on the averaged flow field are mainly determined by the reduction in the velocity dissimilarity over the mixing layer due to the friction on the bottom surface (van Prooijen and Uijttewaal 2002), where the vertical confinement largely affects the large vortical structures and rapidly decreases the number and spectrum of vortices in downstream direction (Shinneeb *et al* 2011).

Furthermore, it is also worth mentioning some of the most notable research that has been conducted on the vortex rebounding from the free surface. In general, the prior literature shows that apart from jet depth from the free surface, there are other factors that affect the association of the jet vorticity to the unrestrained surface in shallow water jets such as, jet angle with the free surface, surface contamination, jet velocity and shape of the jet (Bernal *et al* 1989, Anthony *et al* 1991, Gharib and Weigand 1996, Bernal and Kwon 1989, Archer *et al* 2007). Some of the reported work focuses on the connection and disconnection of a vortex ring advancing towards a free surface obliquely, whereas some deal with normal interaction (Archer *et al* 2007), and others discussthe vortex ring moving parallel to the free surface (Bernal and Kwon 1989). According to (Bernal and Kwon 1989), surface contamination has a profound influence on the behaviour of a single vortex ring. (Bernal *et al* 1989) investigated this phenomenon and reported that even a very small amount of surface active agent in bulk water significantly modifies the dynamics of vortex ring interaction with the free surface because the vorticity diffuses away from the surface and rolls up into secondary vortices, altering the global evolution of the vortex ring. In addition, investigations into the interaction of a laminar two-dimensional vortex pair with clean and contaminated free surfaces shows that rebounding of the primary vortex near the free surface is also possible due to generated secondary vorticity beneath the contaminated surface, but rebounding is absent for clean surfaces (Bernal *et al* 1989). In conclusion, it is worth pointing out here that the interaction of a vortex ring with a free surface is an intriguing problem in fluid dynamics owing to the complicated flow physics surrounding the vortex ring growth, instability and breakdown. In a previous preliminary work, we have studied the detailed characterization of coherent structures in a synthetic jet flow field at various length scales in temporal domain using velocity signal analysis, along with flow visualization (Kumar *et al* 2017). In a following work, we have explored the behavior of synthetic jets at

shallow water depths only at two selected values of Reynolds numbers, and both LIF and LDV measurements were conducted only in a single plane. Clearly, the recorded data was insufficient to understand the physical mechanisms at play (Kumar *et al* 2017b). Thus, a detailed systematic study on the behavior of *synthetic jets* in shallow water depths and the interaction of the formed vortex rings with the free surface needs to be conducted.

Thus, in the current paper, we expand upon our previous work and focus our attention on exploring the effects of Froude number and Reynolds number variation on the evolution and propagation of a submerged synthetic jet in a quiescent fluid medium, ejecting parallel to the unrestrained surface, through detailed qualitative analysis and quantitative measurements in two different planes. The primary objective of these analysis and measurements is to gain a physical insight into the characteristics of vortex ring in synthetic jet ejected from a fixed orifice at different values of Froude number and Reynolds number based on circulation. The current paper is structured as follows: section 2 furnishes the details on the experimental setup and methodology. Thereafter, in section 3, we deal with the results and discussion on flow visualization and time-averaged velocity measurements with a focus on variation with regard to Froude number and circulation based Reynolds number. Finally, the conclusions are presented in section 4.

## 2. Experimental setup and methodology

Experiments are conducted to study the interaction of the vortex rings with the free surface, at different unconfined surface heights ($H$) and actuation frequencies ($f_{\mathrm{act}}$) of the jet. The experiments are carried out in a water tank of dimensions 1000 mm (length) $\times$ 500 mm (width) $\times$ 500 mm (height). The water tank experimental setup is made with 12 mm acrylic sheets, allowing for complete optical view from all sides, with a free water surface that can be treated to be contaminated. The actuator is stationed at the middle of 500 mm $\times$ 500 mm wall in such a way that the spacing between the walls from all sides and the synthetic jet is 250 mm. The orifice diameter ($D$) in the current experiments is 13 mm and the distance from the center of the orifice to bottom and side walls is greater than 19$D$. Prior research on this experimental setup (viz. Kumar and Karn 2018, Kumar *et al* 2019) has suggested the maximum growth of ring size and the maximum spreading of synthetic jet to be 2$D$ and 3.5$D$, respectively and thus the blockage effects can be considered negligible in the present study. The synthetic jet generation unit comprises a circular cavity of inner diameter ($D_{\mathrm{ca}}$) equal to 70 mm and a height of 60 mm. At one extreme of the cavity boundary, an arrangement to install an orifice plate of 3 mm thickness is made and on the opposite end of the cavity a circular diaphragm is attached, which is further interlinked to the electromagnetic actuator through a stainless steel bar. The diaphragm is made of nitrile coated nylon rubber sheet with 1.5 mm thick having a circular steel disc ($D_{\mathrm{cy}}$) of 40 mm diameter at center. A frequency controller unit drives the oscillations of the electromagnetic actuator through a sinusoidal voltage signal. The frequency in the flow field is also obtained from the velocity signal in the vicinity of the diaphragm and is compared with the frequency of the diaphragm measured through the oscilloscope.

The PLIF technique is employed for the qualitative examination of the flow is done. Figure 2(b) illustrates the PLIF imaging plane (or, $XZ$ plane) at the orifice center. $XZ$ plane is chosen as the imaging plane in our experiments, in order to capture the vortex roll-up in the side view. Figure 2(c) further provides details on the PLIF setup. A COHERENT® INNOVA-90, 4 W continuous wave Argon-Ion Laser is used in our experiments with a plano-concave cylindrical lens of focal length (15 mm) to generate a laser sheet of 1.5 mm thickness. The PLIF images are captured with a resolution of 1280 $\times$ 1280 and a frame rate between 10 to 30 fps using a

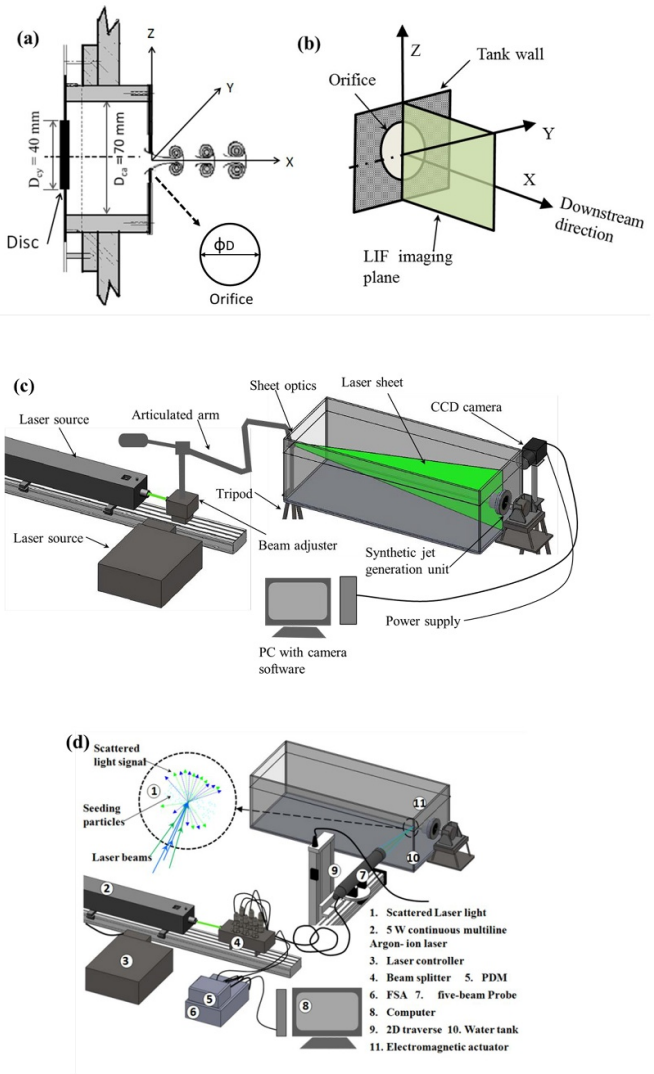


**Figure 2.** Experimental setup (a) showing the cross-sectional view of the cavity, (b) the orientation of axes at the orifice center, (c) for flow visualization using PLIF technique, and (d) for velocity measurement using LDV. (a) and (d) Kumar *et al* 2017b. With permission of Springer.

Basler® A501-KC camera. Fluorescein and Rhodamine (6G) dyes are employed in our experiments. Velocity measurements in the cross streamwise and streamwise direction are carried out using five-beam LDV probe as presented in figure 2(d). Hollow glass spheres coated with silver in the diameter range of 8 $\mu$m–12 $\mu$m are used as external flow seeding particles. At each point, the velocity data is sampled over a minimum 60 operational cycles, and an arithmetic mean is obtained. A maximum fluctuation of $\pm 3.7\%$ around the mean is observed in the measured velocity components considering uneven sampling. The five-beam probe is stationed on a 2D traverse that moves in transverse plane ($YZ$-plane) with a resolution of 6.25 $\mu$m and an accuracy of $\pm 300$ $\mu$m.

The physical parameters involved in the present study are frequency ($f$) and amplitude of oscillation of the actuator ($\Delta$), averaged jet exit velocity ($U_{\mathrm{o}}$), ejection time in a cycle ($T_{\mathrm{e}}$), water free surface height ($H$), orifice diameter ($D$) and the geometrical parameters of the diaphragm such as inner cavity diameter ($D_{\mathrm{ca}}$) and diameter of the disk ($D_{\mathrm{cy}}$). As suggested by (Mohseni 2006), the ejected volume ($V_{\mathrm{d}}$) for the diaphragm can be calculated as $V_{\mathrm{d}} = \pi\Delta/8\left(D_{ca}^2 + D_{cy}^2\right)$. The average jet exit velocity can be calculated as $U_o = V_d/A_oT_e$ where $A_o$ denotes the cross-sectional area of the orifice. In the current setup, since the actuation frequency and the diaphragm displacement are coupled with each other ($\Delta$ varied between 1.2 mm at 1 Hz to 2.2 mm at 6 Hz.), a similar inter-dependence is observed in the Reynolds number and Strouhal number, defined conventionally based on the jet ejection velocity, $U_{\mathrm{o}}$. Therefore, an alternative dimensionless parameter has to be introduced that assimilates the effect of variation in both ejection velocity and actuation frequency. Hence, circulation of the synthetic jet at orifice exit is defined as $\Gamma = \left(\pi^2/128\right)\left(\Delta^2 f\right)\left(D_{ca}/D\right)^4$, similar to (Jabbal *et al* 2006). Next, it may be noted that the generated vortex rings in the current study gain an induced velocity that is dependent on the circulation of the vortex ring. Thus, Reynolds number defined based on circulation is introduced as $Re_\Gamma = \Gamma/\nu$, similar to other prior studies (for instance, Melander and Hussain 1989). Since the flow involves a free water surface and the experiments are conducted at different water depths, Froude number is defined conventionally as $Fr = U_o/\sqrt{gH}$;, where $\nu$ and $g$ represent the kinematic viscosity of water and acceleration due to gravity, respectively. Further, the free surface height and the distances from the center of the orifice are non-dimensionalized with respect to $D$, and are represented as $\tilde{h}$, $\tilde{x}$, $\tilde{y}$ and $\tilde{z}$ respectively. The uncertainty in the frequency of actuation of cam number actuated synthetic jet and of Reynolds number is $\pm 5\%$ and $\pm 5.2\%$, respectively. Table 1 below presents all the values of different non-dimensional parameters at which experiments are conducted.

## 3. Results and discussion

In the present work, the effect of the shallow water on the flow characteristic of synthetic jet is presented at three distinct values of water depths, $\tilde{h}$= 1.5, 3.0 and 5.0 and at four different frequencies. As shown in figure 2(b), the PLIF images are captured in a vertical plane aligned with synthetic jet axis and perpendicular to the free surface of the water. The velocity distributions are measured along the synthetic jet centerline at five different downstream locations ($\tilde{x}$ = 0.5, 2, 5, 8 and 12) in vertical transverse planes (referred hereafter as $XZ$ planes). The terms free surface, unrestrained surface and unconfined surface have been interchangeably used in the current paper.

### 3.1. Flow visualization

In this section, the qualitative analysis of the vortex ring and the free surface interaction is studied through flow visualization. First, the effect of water depths from the unconfined surface (variation in Froude number) and second, the implications of variations in Reynolds number are discussed subsequently. The vortex interaction with the free surface is observed between $\tilde{x} = 10$ to $\tilde{x} = 12$ as shown in figure 3(a). This causes perturbations on the free surface and it has been observed that these perturbations are most dominant at $\tilde{h} = 1.5$. At the same shallow water depth (i.e. $\tilde{h} = 1.5$), as $Re_\Gamma$ is increased from 370 to 875, the vortex ring interacts with the free surface earlier along the $x$-direction, as compared to before. As shown in figure 3(b), the vortex interacts with the free surface between $\tilde{x} = 6$ to 8. In both the cases, vortex ring drifts upwards toward the free surface and the upper counter-rotating vortices of the ring lose its vorticity and disappear earlier than the lower counter rotating vortices. The underlying physics

**Table 1.** Values of the relevant non-dimensional parameters for all experimental conditions at different frequencies and free surface height. Kinematic viscosity of water has been calculated at 25 °C as $1.0 \times 10^{-6}$ m$^2$ s$^{-1}$.

| Frequency of actuation, $f_{act}$ (Hz) | Avg. slug velocity $U_o$ (mm s$^{-1}$) | Diaphragm displacement ($\Delta$ in mm) | $L/D$ | Reynolds number, $Re_\Gamma$ | Froude number $Fr$ | | |
|---|---|---|---|---|---|---|---|
| | | | | | $\tilde{h} = 1.5$ | $\tilde{h} = 3.0$ | $\tilde{h} = 5.0$ |
| 1 | 25.7 | 3.58 | 1.67 | 370 | 0.06 | 0.04 | 0.033 |
| 2 | 56.9 | 4.18 | 2.33 | 845 | 0.13 | 0.09 | 0.073 |
| 4 | 184.2 | 5.93 | 3.03 | 2663 | 0.42 | 0.30 | 0.23 |
| 6 | 407.2 | 8,35 | 4.55 | 5904 | 0.93 | 0.66 | 0.51 |

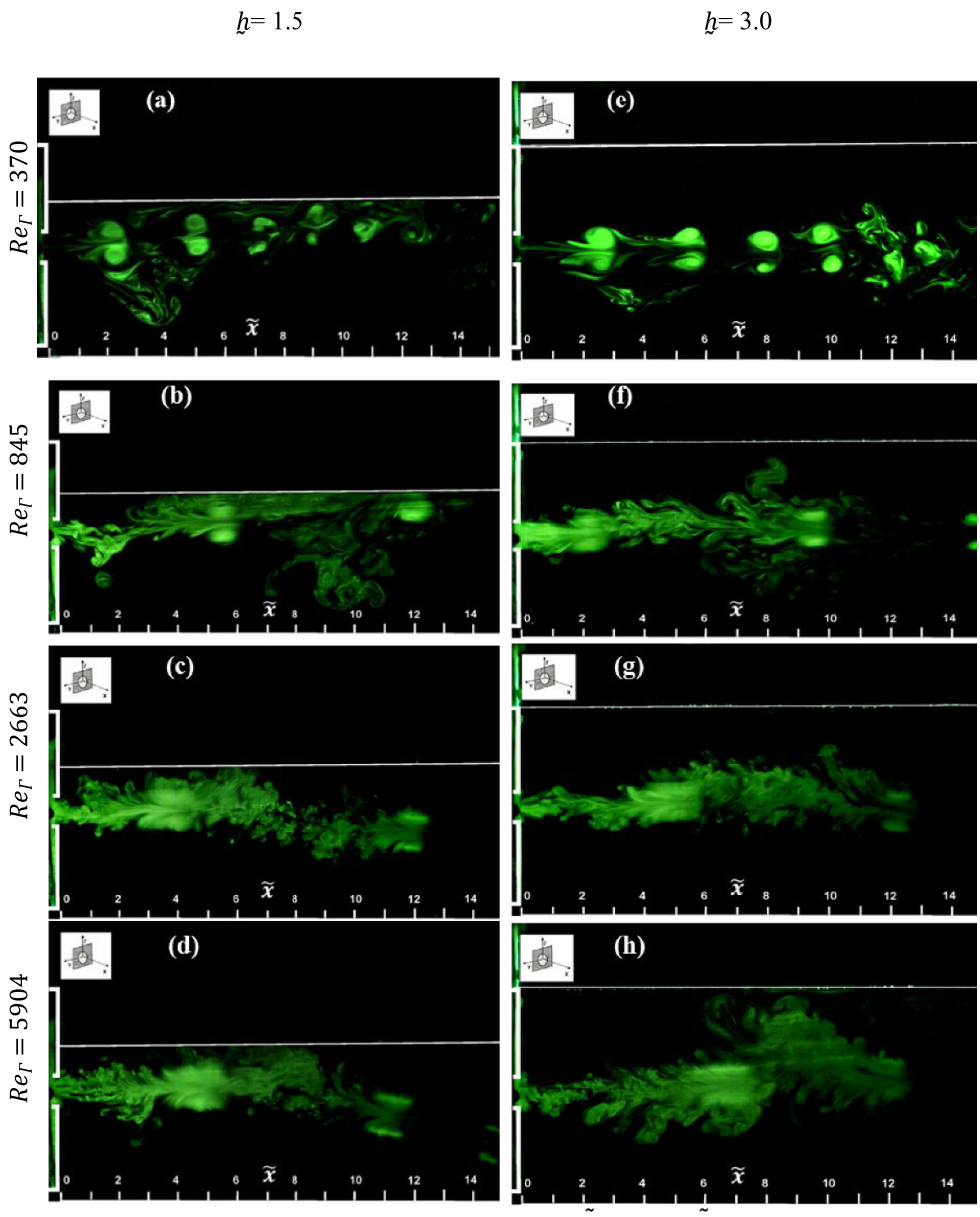


**Figure 3.** Visualization of flow patterns in $XZ$ plane at $\tilde{h} = 1.5$ and $\tilde{h} = 3.0$, Reynolds number varying from $Re_\Gamma = 370$ to 5904 as shown on the left. The horizontal white lines denote the free surface. The red dotted line depicts the average trajectory of trailing and leading vortex rings, obtained from a continuous sequence of images. Figures (a), (b), (d) and (h) Kumar *et al* 2017b. With permission of Springer.

behind this has been well explained by Bernal and Kwon (1989), where it was reported that the association of the vortex rings and the unrestrained surface may result in the curtailment of vortex lines, diminishing the vortex ring upper half that revolves in counter clockwise direction as seen from the cross sectional view.

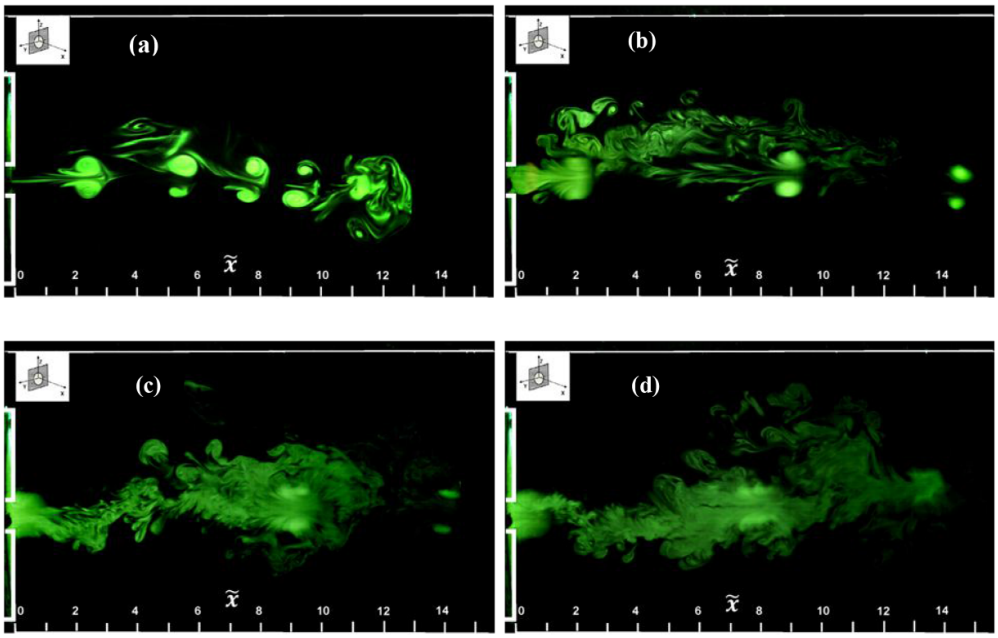


**Figure 4.** Visualization of flow patterns for a synthetic jet in *XZ* plane for $\tilde{h} = 5.0$ at $Re_\Gamma$ equal to (a) 370 (b) 845 (c) 2663 and (d) 5904. The horizontal line on the top denotes the free surface. The red dotted line depicts the trajectory of trailing and leading vortex ring. Figures (a) and (d) Kumar *et al* 2017b. With permission of Springer.

When the momentum of synthetic jet is enhanced further by increasing the $Re_\Gamma$ to 2663 and 5904, the vortex ring moves along its centerline beyond $\tilde{x} = 5$ and $\tilde{x} = 8$ for $Re_\Gamma = 2663$ and 5904, respectively. Further, a striking and interesting observation is that the leading vortex ring rather than interacting with the free surface, takes a curvilinear trajectory, bends and moves away from the free surface. However, the low strength vortices (trailing jet) continues to move upwards, similar to the previouscase. The reason behind this phenomenon could be the formation of a non-symmetric recirculation zone in the vicinity of the jet flow. In general, the synthetic jet creates a larger recirculation zone around it, extended to several diameters downstream. When this recirculation zone is symmetric, the synthetic jet follows the expected path i.e. along its centerline. But when this recirculation zone is non-symmetric, as happens in the case of shallow waters, the synthetic jet trajectory gets altered, depending on the momentum. This may be one of the reasons of vortex core interaction at low $Re_\Gamma = 370$ and 845, whereas the occurrence of rebounding at $Re_\Gamma = 2663$ and 5904.

In figures 3(e)–(h), the non-dimensional water depth, $\tilde{h}$ has been increased from 1.5 to 3. At $Re_\Gamma = 370$ and 845, the vortex rings either moves along or close to the synthetic jet centerline or without interacting with the free surface. However, at $Re_\Gamma = 2663$ and 5904, the leading vortex rings moves upward and shows a curvilinear deflection, although the trailing ring continues to move upward and interact with free surface, somewhere between $\tilde{x} = 8$ to 10. As shown in figure 4, at $\tilde{h}$= 5 the vortex rings moves close to the synthetic jet centerline and no significant variation is observed in the PLIF images at $Re_\Gamma = 370$ and 845. At $Re_\Gamma = 2663$, the trajectory of vortex ring oscillate along the synthetic jet centerline and some undulations are observed, whereas at $Re_\Gamma = 5904$, in the far field region after $\tilde{x} = 8$, the path of leading and trailing vortex rings diverges. Most importantly, this deflection is observed to be not as significant

as compared to $\tilde{h} = 1.5$ case for the attainable range of $Re_\Gamma$ in our experiments. It is indeed possible that even at larger $\tilde{h}$, the deflection of these vortex rings can be observed at higher $Re_\Gamma$. Thus, it can be suggested that the deflection of the vortex rings from the free surface depends not only on $Re_\Gamma$, but possibly also on $Fr$. It can be conjectured that the vortex deflection may be a function of both $Re_\Gamma$ and $Fr$, and a critical value of the product $Re_\Gamma{}^m Fr^n$ (m and n are constants, unique to each $\tilde{h}$) may exist that determine the transition of the vortex ring deflection at each $\tilde{h}$, similar to the upward deflection of twin vortex closure modes in supercavitation physics, that are governed by the value of the product of cavitation number and Froude number (Karn *et al* 2015, 2016). Although a conclusive evidence to substantiate this conjecture on the flow physics of synthetic jets remains to be investigated, some general trends can be observed from our current experiments. For instance, in our experiments at $\tilde{h} = 1.5$, an upward flection of the vortex ring trajectory is observed for $Re_\Gamma Fr$ in the range of 22–110, whereas a downward flection is noticed at much higher $Re_\Gamma Fr$ around 1100–5500. However, to substantiate this hypothesis, further systematic experiments will be required at a much larger range of variation of both $Re_\Gamma$ and $Fr$. Moreover, since all the images shown here are instantaneous snapshots and there are many chaotic effects that may disturb the jet flow, these images cannot qualitatively characterize and completely capture the mechanism behind jet curvature. As mentioned before, the PLIF images are captured after few cycles of synthetic jet actuation, and it is indeed possible that such different trajectories may only happen during the initial stages of the synthetic jet actuation. Therefore, to gain a better insight into the flow physics, the time averaged LDV measurements are also discussed in the next section.

### 3.2. Velocity measurements

In the above section, the shown PLIF images reveal only the qualitative nature of the vortex ring. The PLIF images are indicative of the instantaneous flow field, and may be affected by attenuation of laser sheet intensity across flow the field. Therefore, velocity measurements are also carried out in the $XZ$ plane using LDV to analyze the flow behavior quantitatively.

*3.2.1. Time averaged velocity in the XZ plane.* Similar to the velocity distribution along the centerline, time averaged velocity distribution for $\tilde{h} = 1.5$ (figure 5(a)) in $XZ$ plane shows the shifting of streamwise velocity towards the free surface. In the near vicinity, or $\tilde{x} = 0.5$, the unrestrained surface has no substantial effect. At $\tilde{x} = 2$, the velocity distribution is relatively symmetrical, although the axis of symmetry is shifted upwards. In the far field, velocity distribution is unsymmetrical about the centerline of the synthetic jet and drifts upwards. The cross stream velocity distribution in figure 5(b) shows a strong upward movement of vortex ring at $\tilde{x} = 0.5$, which is quite negligible as observed between $\tilde{x} = 2$ to 5. Between $\tilde{x} = 8$ to 12, a strong upward movement of fluid is observed due to vortex interaction and final breakdown at free surface can be seen in figure 3(a). For $\tilde{h} = 3$ and $\tilde{h} = 5$, flow is akin to a deeply submerged jet and the unconfined surface has a very minimal impact on the velocity distribution. A backflow zone with negative velocity is realized in the near field at $\tilde{x} = 0.5$ around the orifice boundary due to the generation of a slight suction in all cases. Again, a symmetry to both sides can be observed as far as this backflow region is concerned and no notable influence of the free surface is evident here. In contrary to $Re_\Gamma = 845$, in figures 5(c) and (d) at $Re_\Gamma = 2663$, the velocity distribution is skewed downwards as seen by the downward movement of synthetic jet in figure 5(d).

In figure 5(b) at $Re_\Gamma = 845$, the distribution of cross stream velocity shows only the upward movement of fluid at $\tilde{x} = 0.5$ between $-1 \leq \tilde{z} \leq 0.4$. At the same location $\tilde{x} = 0.5$ for $Re_\Gamma = 2663$ in figure 5(d), the downward as well as upward movement of fluid is observed between

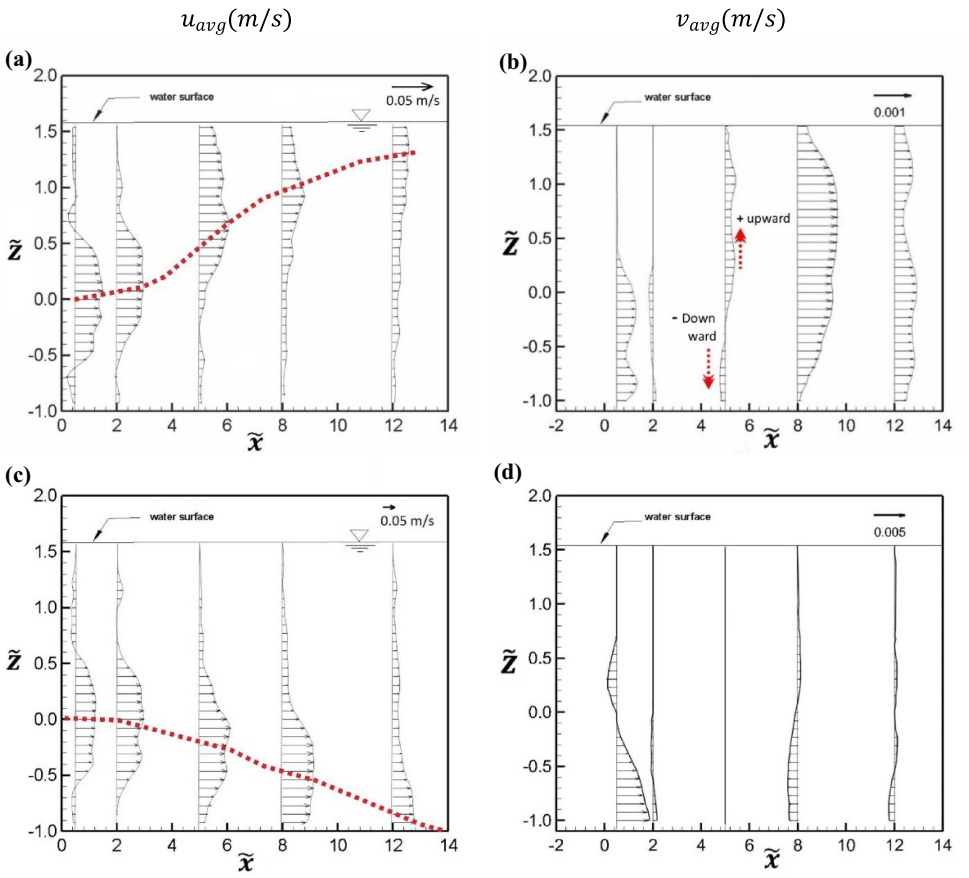


**Figure 5.** Time averaged stream-wise velocity and their corresponding cross stream velocity distribution for a shallow water depth of $\tilde{h} = 1.5$ at $Re_\Gamma$ equal to (a, b) 845 and (c, d) 2663. (The upward ($+v_{avg}$) and downward ($-v_{avg}$) movement of fluid are shown by dotted arrow. The red dotted lines are obtained by connecting the velocity maxima, to compare the vortex trajectory at different $Re_\Gamma$..

$-0.3 \leq \tilde{z} \leq 0.5$ and $-1 \leq \tilde{z} \leq -0.3$ respectively. Since this region lies in the suction zone of the synthetic jet (less than $\tilde{x} = 2$), the suction stroke combined with the shallow water depth affects the formation and propagation of vortex ring. The cross stream velocity distribution at $Re_\Gamma = 845$ and $Re_\Gamma = 2663$ shown in figures 5(b) and (d) are opposite to each other at $\tilde{x} = 8$ and 12 supporting the observation in the image shown in figure 3. Figures 6 and 7 show the time averaged velocity distribution of synthetic jet at water depth equal to $\tilde{h} = 3$ and 5. In figures 6(a) and (c), as compared to the above cases no significant changes in the stream wise velocity distribution of synthetic jet is observed at $Re_\Gamma = 845$ and $Re_\Gamma = 2663$ except that the profile is more symmetric $Re_\Gamma = 2663$ in comparison to $Re_\Gamma = 845$. In figures 6(b) and (d), the trend of cross stream velocity distribution is similar at $\tilde{x} = 0.5$ and at $\tilde{x} = 2$ for $Re_\Gamma = 845$ and having inversion point at $\tilde{z} = -0.3$ and $-0.62$ respectively at $\tilde{x} = 0.5$. The far field has a chaotic upward and downward movement of fluids except at $\tilde{x}$= 5 for $Re_\Gamma = 845$, where a significant downward motion is observed between $\tilde{z} = 0.6$ and 1.8.

In figures 7(a) and (b), the streamwise velocity distribution is symmetric about the jet centerline at all downstream locations for both the Reynolds numbers. The magnitude of the

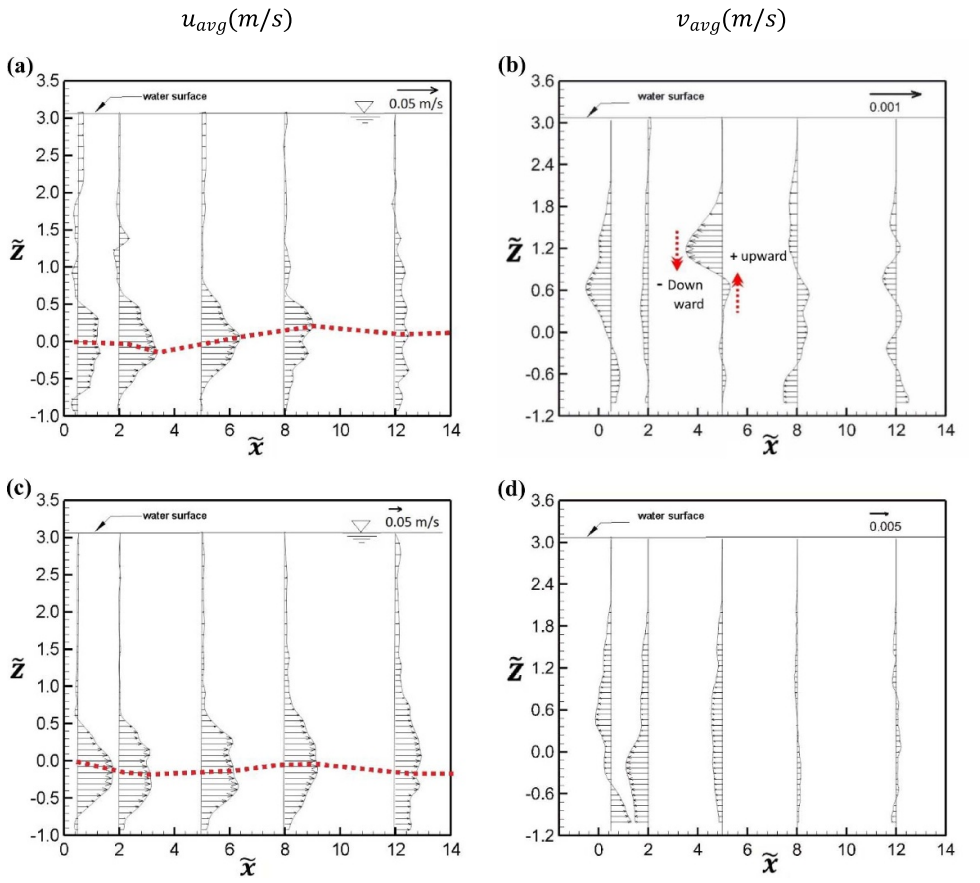


**Figure 6.** Time averaged stream-wise velocity and their corresponding cross stream velocity distribution for a shallow water depth of $\tilde{h} = 3.0$ at $Re_\Gamma$ equal to (a), (b) 845 and (c), (d) 2663. (The upward ($+v_{avg}$) and downward ($-v_{avg}$) movement of fluid are shown by the dotted arrow.

cross stream velocity also varies close to the synthetic jet centerline. Therefore it can be concluded that at $\tilde{h} = 5$, the free surface has a negligible effect on the flow pattern of the synthetic jet. In summary, the time averaged velocity flow field of synthetic jet in shallow water at different depths $\tilde{h} = 1.5$, 3 and 5 are shown in figures 5–7 for $Re_\Gamma = 845$ and $Re_\Gamma = 2663$. At $\tilde{h} = 1.5$, vortex ring drifts upwards and an interaction of upper counter rotating vortices with the unrestrained surface is noted at $Re_\Gamma = 845$ andrebounding of the vortex ring near the free surface in far-field is observed at $Re_\Gamma = 2663$.

*3.2.2. Time averaged velocity along synthetic jet centerline.* The time-averaged streamwise velocity ($u_{\text{avg}}$) and cross-stream velocity ($v_{\text{avg}}$) along the synthetic jet centerline at three different non-dimensional water depths of $\tilde{h} = 1.5$, 3 and 5 are measured for four different values of $Re_\Gamma = 370$, 845, 2663 and 5904. The velocity field is studied by non-dimensionalizing the streamwise and cross-stream velocity by the corresponding slug velocity ($U_{\text{o}}$). The slug velocity is defined as the average ejection velocity of expelled fluid through the orifice during the forward stroke of the diaphragm. Figure 8 illustrates the variation of the non-dimensional

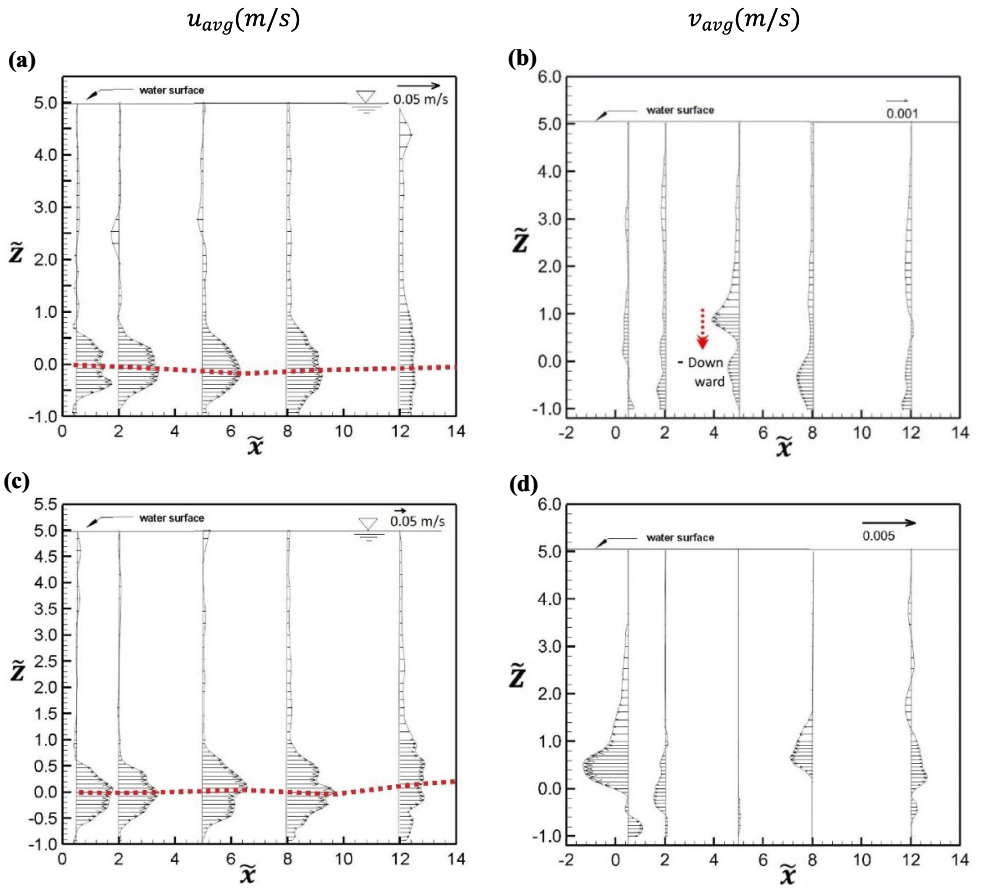


**Figure 7.** Time averaged stream-wise velocity and their corresponding cross stream velocity distribution for a shallow water depth of $\tilde{h} = 5.0$ at $Re_\Gamma$ equal to (a), (b) 845 and (c), (d) 2663. (The upward ($+v_{avg}$) and downward ($-v_{avg}$) movement of fluid are shown by the dotted arrow.

streamwise velocity and the non-dimensional cross-stream velocity at different transverse distances. As shown in figure 8, the overall value of $u_{\text{avg}}/U_{\text{o}}$, is lowest for $Re_\Gamma = 5904$ and highest for $Re_\Gamma = 370$. This is because, increasing the frequency increases the slug velocity and also changes the velocity distribution across the orifice. The increment in the time averaged velocity along the centerline is slower than the slug velocity due to widening of the suction region from the periphery of the orifice towards the center at an increased $Re_\Gamma$. Since the slug velocity remains constant at a particular $Re_\Gamma$, the profile of the curves in figure 8 is a function of $u_{\text{avg}}$ and $v_{\text{avg}}$ only.

In figure 8(a) for $\tilde{h} = 1.5$, the streamwise velocity of synthetic jet at an $Re_\Gamma = 370$ decline sharply in magnitude due to the upward movement of vortex ring towards the free surface as evident in the distribution of cross stream velocity shown in figure 8(b). At an $Re_\Gamma = 845$, the peak of cross stream velocity gets shifted to $\tilde{x} = 3$ with reduced magnitude in comparison to $Re_\Gamma = 370$, which gives a reduced slope for streamwise velocity distribution. However, at both the $Re_\Gamma$, the vortex ring moves upward and interacts with the free surface and finally disappears by losing its vorticity. At greater circulations such as $Re_\Gamma = 2663$ and $Re_\Gamma = 5904$,

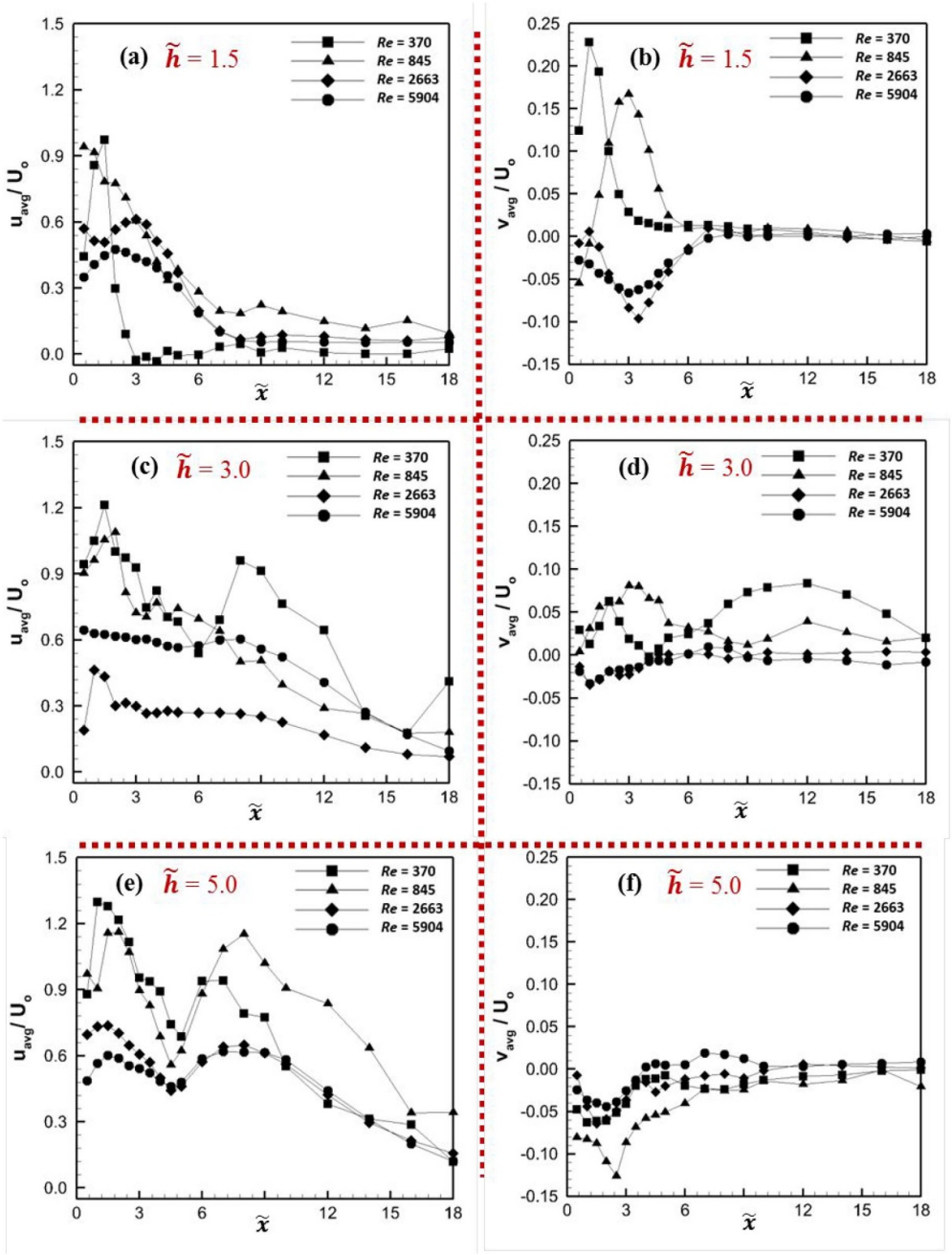


**Figure 8.** Non-dimensional time averaged stream wise and cross-stream velocity with respect to transverse distance at (a), (b)$\tilde{h} = 1.5$, (c), (d) $\tilde{h} = 3.0$, and (e), (f) $\tilde{h} = 5.0$ at different $Re_\Gamma$. (Note that $Re_\Gamma$ has been denoted as $Re$ for the sake of brevity.).

the synthetic jet behavior differs due to vortex rebounding from the free surface (see figures 3(c) and (d)). This trend is in response to the negative value of cross stream velocity in figure

8(b) between $\widetilde{x} = 0$ to 6, which is just opposite to the trend observed at $Re_\Gamma = 370$ and $Re_\Gamma = 854$. Similar observation is also found in figure 8(c) for an increased water depth until $\tilde{h} = 3$ with an oscillating value of $u_{avg}$. In figure 8(d), the absolute value of the cross stream velocity at all four $Re_\Gamma$ decreases in comparison to the above case, indicating that the effect of the free surface is reduced at this depth. When the free surface height is increased to $\tilde{h} = 5.0$, the velocity distribution trends are similar at all the values of $Re_\Gamma$, as shown in figures 8(e) and (f).

It has been observed from PLIF images and the centerline velocity distributions that the synthetic jet shows similar trends at lower Reynolds numbers of $Re_\Gamma = 370$ and 845, but the behavior gets altered at higher value of $Re_\Gamma$ such as 2663 and 5904. Since the behavior at the extreme frequencies (i.e. $Re_\Gamma = 370$ and $Re_\Gamma = 5904$) has already been reported in a recent study (Kumar *et al* 2017b), we focus our attention only on the intermediate Reynolds number range, i.e. $Re_\Gamma = 845$ and $Re_\Gamma = 2663$, while presenting the cross-stream velocity distribution in the following section.

Finally, it is also worth mentioning the reasons behind some of the apparent differences behind the instantaneous PLIF images and the trends observed from the time-averaged LDV measurements. Although the PLIF clearly shows the different trajectories of the leading and trailing vortex rings, no such observation can be made from the time-averaged velocity measurements. The reason behind the different trajectories can be attributed to the accumulation of initiating vortex rings, which sometimes follow a slightly different path than the following train of vortex ring due partly to the variation in the local flow field. Also, some differences between the PLIF measurements and the LDV measurements is obvious since the former is instantaneous while the latter entails time-averaging. For instance, the trailing vortex ring, which is visible in the PLIF, is not evident in the time-averaged LDV measurements because of its extremely low velocities as compared to that of leading vortex rings. Clearly, it is also possible that such different trajectories may only occur only during the initial stages of the synthetic jet actuation. Indeed, more controlled experiments (such as Time-resolved PIV measurements) are required to ascertain the phenomenon under question. In fact, the deflection of these vortex rings is a three-dimensional phenomenon and any systematic study into this necessitates that the entire three-dimensional flow physics be captured, to arrive at some substantial conclusions. Yet, in spite of these limitations that may show some slight differences between LDV and PLIF due to the above-mentioned reasons, the current study clearly presents a systematic investigation of shallow submerged synthetic jets and reports the occurrence of hitherto unreported phenomenon of vortex rebounding from the free surface, as evidenced by the LDV measurements, and also captured using PLIF visualizations. To fully understand the mechanisms involved in the vortex interaction and rebounding at free surface, a time resolved velocity flow field analysis and PLIF is required in both the transverse planes, which could not be carried out in the current study because of experimental limitations and probably could be taken up by future studies.

## 4. Conclusions

The interaction of a submerged shallow synthetic jet with a parallel free surface is of considerable interest because of its relevance to the operation of marine vehicles. In the current study, we explore a submerged synthetic jet ejecting laterally to the free surface in motionless flow through PLIF and LDV measurements, to gain a physical insight into the characteristics of vortex ring in synthetic jet ejected from a fixed orifice at different water depths and various actuation frequencies of the jet. Experiments are carried out for three distinct non-dimensional

free surface heights of 1.5, 3 and 5 from the centerline of the orifice, and at value of Reynolds number based on circulation in the range of 370–5904. It was found that at shallow water depths such as $\tilde{h} = 1.5$, vortex rings gravitate to the unrestrained surface at lower value of Reynolds number of 370 and 845, but bounce back and move away from the free surface at greater values of Reynolds number 2663 and 5904. The results also show no significant impact of the free surface on the formation and propagation of synthetic jet at greater non-dimensional water depths of $\tilde{h} = 3$ and $\tilde{h} = 5$ in the range of Reynolds number attainable in our experiments. At high $Re_\Gamma$, both the leading and trailing vortex rings are visible in the PLIF images, although the trailing vortex is not visible in the LDV measurements, because of time-averaging, that nullifies the low velocity as compared to the leading vortex ring. It is concluded that the vortex rings may interact or rebound from the free surface depending on its circulation strength (or circulation Reynolds number) and non-dimensional water depth.

## Acknowledgments

The first author gratefully acknowledges the contribution of Professor P K Panigrahi and Professor A K Saha for their support and guidance in carrying out the experiments at IIT Kanpur. We also thank Mr Sri Ragunath V for his assistance in the preparation of this manuscript.

## ORCID iD

Ashish Karn https://orcid.org/0000-0003-0671-4285

## References

Al-Atabi M 2011 Experimental investigation of the use of synthetic jets for mixing in vessels *J. Fluids Eng.* **133**

Amitay M, Honohan A, Trautman M and Glezer A 2004 Modification of the aerodynamics characteristics of bluff bodies using fluidic actuators *AIAA*

Amitay M, Pitt D and Glezer A 2002 Seperation control in duct flows *J. Aircr.* **39** 616–20

Amitay M, Smith D R, Kibens V, Parekh D E and Glezer A 2001 Modification of the aerodynamics characteristics of an unconventional airfoil using synthetic jet actuators *AIAA J.* **39** 361–70

Anthony D G, Hirsa A and Willmarth W W 1991 On the interaction of a submerged turbulent jet with a clean or contaminated free surface *Phys. Fluids* **3** 245

Archer P J, Thomas T, Yorke C P and Coleman G N 2007 Numerical study of vortex ring evolution and interaction with a free surface *5th Int. Symp. on Turbulence and Shear Flow Phenomena*

Bernal L P, Hirsa A, Kwon J T and Willmarth W W 1989 On the interaction of vortex rings and pairs with a free surface for varying amounts of surface active agent *Phys. Fluids A Fluid Dyn.* **1** 2001–4

Bernal L P and Kwon J T 1989 Vortex ring dynamics at a free surface *Phys. Fluids Fluid Dyn.* **1** 449–51

Buren V T, Leong C and Whalen E 2016 Impact of orifice orientation on a finite-span synthetic jet interaction with a crossflow *Phys. Fluids* **28** 1–20

De Luca L, Girfoglio M and Coppola G 2014 Modeling and experimental validation of the frequency response of synthetic jet actuators *AIAA J.* **52** 1733–48

Feng L-H and Wang -J-J 2012 Synthetic jet control of separation in the flow over a circular cylinder *Exp. Fluids* **53** 467–80

Freund J B and Moin P 2000 Jet mixing enhancement by high-amplitude fluidic actuation *AIAA J.* **38** 1863–70

Fung P and Amitay M 2002 Active flow control application on a mini ducted fan UAV *J. Aircr.* **39** 561–71

Gharib M and Weigand A 1996 Experimental studies of vortex disconnection and connection at a free surface *J. Fluid Mech.* **321** 59–86

Gil P and Strzelczyk P 2016 Performance and efficiency of loudspeaker driven synthetic jet actuator *Exp. Therm. Fluid Sci.* **76** 163–74
Glezer A, Amitay M and Honohan A 2005 Aspects of low- and high-frequency actuation for aerodynamic flow control *AIAA J.* **43** 1501–11 (accepted for publication)
Jabbal M, Wu J and Zhong S 2006 The performance of round synthetic jets in quiescent flow *Aeronaut. J.* **110** 385–93
Jagadeesh P, Murali K and Idichandy V 2009 Experimental investigation of hydrodynamic force coefficients over AUV hull *Ocean Eng.* **36** 113–8
Karn A, Arndt R E A and Hong J 2016 An experimental investigation into supercavity closure mechanisms *J. Fluid Mech.* **789**
Karn A, Arndt R E A and Hong J 2015 Dependence of supercavity closure upon flow unsteadiness *Exp. Therm. Fluid Sci.* **68**
Kumar A, Gupta M, Saha A K and Panigrahi P K 2017b Effect of free surface on submerged synthetic jet parallel to the surface *Fluid Mechanics and Fluid Power–Contemporary Research* (Berlin: Springer) pp 53–61
Kumar A and Karn A 2018 Qualitative and quantitative characterization of a synthetic jet mounted on a convex torpedo-like surface under cross-flow *Int. J. Heat Fluid Flow* **74** 198–208
Kumar A, Saha A K, Panigrahi P K and Karn A 2019 On the flow physics and vortex behavior of rectangular orifice synthetic jets *Exp. Therm. Fluid Sci.* **103** 163–81
Kumar A, Saha A K and Panigrahi P K 2017 Time–frequency analysis of submerged synthetic jet *Fluid Dyn. Res.* **49** 065510
Laouedj S, Solano J P and Benazza A 2015 Synthetic jet cross-flow interaction with orifice obstruction *Int. J. Numer. Methods Heat Fluid Flow* **25** 749–61
Lardeau S and Leschziner M A 2011 The interaction of round synthetic jets with a turbulent boundary layer separating from a rounded ramp *J. Fluid Mech.* **683** 172–211
Linden P F and Turner J S 2004 Optimal vortex rings and aquatic propulsion mechanisms *R. Soc.* **271** 647–53
Mcguinn A, Farrelly R, Persoons T and Murray D B 2013 Flow regime characterization of an impinging axisymmetric synthetic jet *Exp. Therm. Fluid Sci.* **47** 241–51
Melander M V and Hussain F 1989 Cross-linking of two antiparallel vortex tubes *Phys. Fluids A Fluid Dyn.* **1** 633–6
Mohseni K and Mittal R 2015 *Synthetic Jets, Fundamentals and Applications* (CRC Press, Taylor & Francis Group)
Mohseni K 2006 Pulsatile vortex generators for low-speed maneuvering of small underwater vehicles *Ocean Eng.* **33** 2209–23
Pavlova A and Amitay M 2006 Electronic cooling using synthetic jet impingement *J. Heat Transfer* **128** 897–907
Rodi W 1982 *Turbulent Buoyant Jets and Plumes. HMT: The Science & Applications of Heat and Mass Transfer. Reports, Reviews & Computer Programs* (Amsterdam: Elsevier)
Shinnee A, Bugg J D and Balachandar R 2011 Coherent structures in shallow water jet *J. Fluids Eng.* **133** 1–14
Smith B and Glezer A 2002 Jet vectoring using synthetic jets *J. Fluid Mech.* **458** 1–34
Smith B L and Swift G W 2003 A comparison between synthetic jets and continous jets *Exp. Fluids* **34** 467–72
Travnicek Z, Nemcova L, Kordik J, Tesar V and Kopecky V 2011 Axisymmetric impinging jet excited by a synthetic jet system *Int. J. Heat Mass Transfer* **55** 1279–90
van Prooijen B C and Uijttewaal W S J 2002 A linear approach for the evolution of coherent structures in shallow mixing layers *Phys. Fluids* **14** 4105–14